## Title

A FLOW-THROUGH POROUS ELECTRODE MODEL: APPLICATION TO METAL-ION REMOVAL FROM DILUTE STREAMS



## Author

Trainham, James A.

## Publication Date

1977

Submitted to Journal of the
Electrochemical Society

LBL-6041
Preprint c. 1

# A FLOW-THROUGH POROUS ELECTRODE MODEL: APPLICATION TO METAL-ION REMOVAL FROM DILUTE STREAMS

James A. Trainham and John Newman



January 1977

Prepared for the U. S. Energy Research and
Development Administration under Contract W-7405-ENG-48



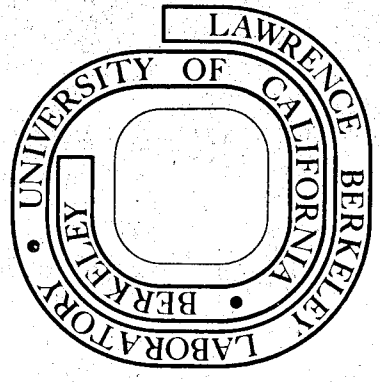

## DISCLAIMER

LBL-6041

# A Flow-Through Porous Electrode Model: Application to Metal-Ion Removal from Dilute Streams

James A. Trainham and John Newman

Materials and Molecular Research Division, Lawrence Berkeley Laboratory, and Department of Chemical Engineering, University of California, Berkeley, California 94720

January, 1977

## Abstract

A one-dimensional model for flow-through porous electrodes operating above and below the limiting current of a metal deposition reaction has been developed. The model assumes there is one primary reactant species in an excess of supporting electrolyte and that a simultaneous side reaction may occur. The model predicts nonuniform reaction rates due to ohmic, mass-transfer, and heterogeneous kinetic limitations; the effects of axial diffusion and dispersion are included. Results are compared with the experimental data observed by various authors for the deposition of copper from sulfate solutions with the simultaneous generation of dissolved hydrogen. Satisfactory agreement between model predictions and experimental data on overall reactor performance and deposit distributions has been accomplished. For an upstream counterelectrode, distributions of reaction rate (for both single and multiple reactions), concentration, and potential describe the detailed system behavior.

Key words: current distribution, potential distribution, mass transfer, axial dispersion, side reaction

## Introduction

Recent publications[1-8] show that flow-through porous electrodes can remove heavy metals from dilute streams, and direct comparisons[9-11] with other electrode systems (fluidized bed electrodes and parallel plate electrodes) show that flow-through porous electrodes can perform better. However, before they are used commercially it must be demonstrated that they can compete successfully with other established processes (e.g., foam fractionation, ion-exchange, precipitation, and cementation). To help design better flow-through porous electrodes so they can compete with these other processes, more sophisticated models are required.

In previous work,[1,12-15] a flow-through porous electrode operating at the limiting current was treated. Sioda[16] gave an analysis for a flow-through porous electrode operating below the limiting current for a reversible reaction described by the Nernst equation, which also includes treatment of the interfacial mass-transfer resistance. Alkire and Gracon[13] included a very general analysis of a single electrode reaction below the limiting current, including the effects of axial diffusion; results are given for an upstream counterelectrode. Recently, Alkire and Gould[17] have extended this work to multiple reaction sequences, which includes: deposition of several metals, deposition of a metal in the presence of a re-dox system, and an ECE sequence applicable to electro-organic synthesis; results are given for a downstream counterelectrode. Ateya and Austin[18] give an analysis similar to Sioda[16] for a single electrode reaction described

by the Nernst equation and study the effects of axial diffusion and dispersion under conditions when the interfacial mass-transfer resistance appears to be negligible.

The present analysis complements previous work by predicting nonuniform reaction rates due to ohmic, mass-transfer, and heterogeneous kinetic limitations in the presence of a side reaction. Also included are the effects of axial diffusion and dispersion without simplification of the Danckwerts,[19] Werner-Wilhelm[20] boundary conditions as was done in previous work.[13,17] Simplifications made possible in the treatment of the side reaction due to the small reactant concentration and the desire to operate at high current efficiencies should make this analysis attractive for design purposes.

## Model

The case of metal-ion removal from dilute streams using a flow-through porous electrode with parallel current and fluid flow can be modeled with the following restrictions:

1) The model is one-dimensional.

2) The porous cathode is of length $L$ and has an isotropic porosity $\varepsilon$ and specific surface area $a$ which remain constant in time.

3) The hydrodynamics are characterized by the superficial velocity $v$ and an average mass-transfer coefficient $k_m$, where axial diffusion and dispersion account for deviations from plug-flow.

4) There is one reactant species in excess supporting electrolyte.

5) A simultaneous side reaction may occur, which is characterized by its rate at the half-wave potential of the primary reaction. Also, if the side reaction involves generation of a gas, it is assumed that the gas will remain in solution so that the velocity profile will not be disturbed.

6) The conductivity of both the matrix and pore solution phases is uniform.

Assumptions 1 through 3 simplify the calculational procedure and are necessary due to the lack of a better description of the complex porous geometry. The validity of assumptions 4 through 6 rests on the small reactant concentration. As a consequence of assumptions 4 and 5, the current efficiency should be high, which further simplifies the model by removing the need to follow any reactant species concentration which participates in the side reaction. This approach emphasizes the salient features of the interaction between the unwanted side reaction and the metal deposition reaction.

## Analysis

The equations which describe the behavior of porous electrodes have been reviewed recently by Newman and Tiedemann.[12]

Only one material balance is required -- that for the metal-ion reactant. At steady-state, this may be expressed as

$$\frac{dN_R}{dx} = a\, j_{Rn} \,, \qquad [1]$$

where in the absence of migration effects the superficial flux $N_R$ of the metal-ion reactant in the direction of the fluid flow is given by

$$N_R = -\varepsilon(D_R + D_a)\frac{dc_R}{dx} + c_R v \ , \qquad [2]$$

and the local pore-wall flux to the flowing solution is related to the average mass-transfer coefficient $k_m$ (corrected for axial diffusion and dispersion[14]) by

$$j_{Rn} = k_m(c_{Rw} - c_R) \ . \qquad [3]$$

The quantities $c_{Rw}$ and $c_R$ are the wall concentration and the pore-solution concentration of the metal-ion reactant averaged over the volume of the pores. In equation 2, $D_R$ is the effective diffusion coefficient of the metal-ion reactant within the pore solution and represents a correction to the molecular diffusion coefficient $D_o$ for tortuosity ($D_R = D_o/\tau^2$, where $\tau$ is the tortuosity factor). $D_a$ is the axial dispersion coefficient taken to be[14]

$$D_a = \frac{3v}{a\varepsilon}(1 - \varepsilon) \ , \qquad [4]$$

which is a fit of a large number of data correlated by Sherwood et al.[21] (see also reference 12).

In the matrix phase, the transport of electrons is governed by Ohm's law

$$i_1 = -\sigma \, d\Phi_1/dx \ . \qquad [5]$$

Since it has been assumed that the concentration of the limiting reactant is small compared to the supporting electrolyte concentration, the diffusion potential is neglected; consequently, the current density $i_2$ in the solution phase is governed by Ohm's law

$$i_2 = -\kappa \, d\Phi_2/dx \ , \qquad [6]$$

where $\kappa$ is the effective conductivity of the solution within the pores, related to the bulk conductivity $\kappa_o$ as follows[22]

$$\kappa = \kappa_o \varepsilon^{1.5} \ . \qquad [7]$$

A consequence of electroneutrality is that charge is conserved between the matrix and pore-solution phases. Mathematically this means the divergence of the total current is zero

$$\frac{di_1}{dx} + \frac{di_2}{dx} = 0 \ . \qquad [8]$$

The transfer current is due to the sum of the individual electrode reactions:

$$\frac{di_2}{dx} = \sum_j a \, i_{nj} \ , \qquad [9]$$

where $i_{nj}$ is the average transfer current density (from the matrix phase to the pore solution phase) due to reaction $j$ in an electrode reaction of the form

$$\sum_i s_{ij} M_i^{z_i} \rightarrow n_j e^- \quad . \qquad [10]$$

With the assumption that the principal reactant $R$ participates only in the primary reaction, we can write

$$i_{nR} = - \frac{nF}{s_R} j_{Rn} = \frac{nF}{s_R} k_m (c_R - c_{Rw}) \quad . \qquad [11]$$

For the case under consideration, the mass-transfer resistance is unimportant for the side reaction, and substitution of equation 11 into equation 9 yields

$$\frac{di_2}{dx} = - \frac{anF}{s_R} j_{Rn} + a\, i_{nS} \quad , \qquad [12]$$

where the subscript $S$ refers to the side reaction.

In general, the average transfer current density due to reaction $j$ may be approximated by the Butler-Volmer equation

$$i_{nj} = i_{oj} \left[ \exp \left( \frac{\alpha_{aj} F}{RT} \eta_{sj} \right) - \exp \left( - \frac{\alpha_{cj} F}{RT} \eta_{sj} \right) \right] \quad , \qquad [13]$$

where $i_{oj}$ is the exchange current density which is assumed to have a composition dependence of the form

$$i_{oj} = i_{oj,ref} \prod_i \left( \frac{c_{iw}}{c_{i,ref}} \right)^{\gamma_{ij}} , \qquad [14]$$

where $i_{oj,ref}$ is the value of the exchange current density for reaction $j$ at a reference composition $c_{i,ref}$. It was further assumed that the transfer coefficients $\alpha_{aj}$ and $\alpha_{cj}$ sum to $n_j$ (a positive number, see equation 10) and that the exponents $\gamma_{ij}$ have the form

$$\gamma_{ij} = q_{ij} + \frac{\alpha_{ij}}{n_j} s_{ij} , \qquad [15]$$

such that $q_{ij} = -s_{ij}$ for a cathodic reactant and zero otherwise.

In equation 13, the surface overpotential for reaction $j$ is given by

$$\eta_{sj} = \Phi_1 - \Phi_2 - U_{jw} , \qquad [16]$$

where

$$U_{jw} = U_j^\theta - U_r^\theta - \frac{RT}{n_j F} \sum_i s_{ij} \ln \frac{c_{iw}}{\rho_o} + \frac{RT}{n_r F} \sum_i s_{ir} \ln \frac{c_{ir}}{\rho_o} , \qquad [17]$$

which is the theoretical open-circuit potential for reaction $j$ at the local wall composition relative to a reference electrode of a given kind, where the subscript $r$ refers to the reference electrode compartment. (The pure-solvent density $\rho_o$ should be expressed in $kg/cm^3$ if the concentrations are given in $mole/cm^3$.)

For the case of metal-ion removal from dilute streams, equations 13 through 17 can be simplified greatly. Let the reference electrode be of the same kind as the metal deposition reaction, where the concentration of the primary reactant in the reference electrode compartment $c_{Rr}$ and the reference concentration in equation 14 $c_{R,ref}$ are set equal to $c_{Rf}$ (the upstream feed concentration of the metal-ion reactant). Also assume that the stoichiometric coefficient $s_R = -1$ . Then equation 13 for a metal deposition reaction reduces to

$$i_{nR} = i_{oR,ref}\left\{\exp\left[\frac{\alpha_{aR}F}{RT}(\Phi_1 - \Phi_2)\right] - \frac{c_{Rw}}{c_{Rf}}\exp\left[-\frac{\alpha_{cR}F}{RT}(\Phi_1 - \Phi_2)\right]\right\} . \quad [18]$$

For a simultaneous side reaction, such as the decomposition of the solvent, equation 13 reduces to an even simpler form

$$i_{nS} = i_{oS,ref}\left\{\exp\left[\frac{\alpha_{aS}F}{RT}(\Phi_1 - \Phi_2 - \Delta U)\right] - \exp\left[-\frac{\alpha_{cS}F}{RT}(\Phi_1 - \Phi_2 - \Delta U)\right]\right\}, \quad [19]$$

where $\Delta U$ is the difference in the theoretical open-circuit potentials of the side reaction and the primary reaction ($\Delta U = U_S - U_R$) at the reference concentrations, which in this case are at the upstream feed composition. Note that any explicit dependence of the rate of the side reaction on the composition has been ignored. This assumption is justified if the current efficiency is high and the ratio of the metal-ion reactant to the reactant species involved in the side reaction (e.g., the hydrogen ion) is small.

Let $\eta = \Phi_1 - \Phi_2$ be defined as the local overpotential, and combine equations 5 and 6:

$$d\eta/dx = d(\Phi_1 - \Phi_2)/dx = -i_1/\sigma + i_2/\kappa \; . \quad [20]$$

The elimination of $c_{Rw}$ between equations 3 and 18 yields

$$j_{Rn} = -\frac{\frac{c_R}{c_{Rf}} - \exp\left[(\alpha_{aR} + \alpha_{cR})F\eta/RT\right]}{\frac{1}{c_{Rf}k_m} - \frac{nF}{s_R i_{oR,ref}}\exp\left[\alpha_{cR}F\eta/RT\right]} \; . \quad [21]$$

Next combine equations 1, 2, and 21 to eliminate $N_R$ and $j_{Rn}$, which results in a material balance equation for the limiting reactant with unknowns $c_R$ and $\eta$ :

$$v\frac{dc_R}{dx} = (D_R + D_a)\frac{d^2c_R}{dx^2} - a\frac{\frac{c_R}{c_{Rf}} - \exp\left[(\alpha_{aR} + \alpha_{cR})F\eta/RT\right]}{\frac{1}{c_{Rf}k_m} - \frac{nF}{s_R i_{oR,ref}}\exp\left[\alpha_{cR}F\eta/RT\right]} \quad . \quad [22]$$

An equation for the potential distribution results from elimination of $i_1$, $i_2$, and $i_{nS}$, between equations 8, 12, 19, 20, and 21 by differentiating equation 20:

$$\frac{d\eta^2}{dx^2} = \left(\frac{1}{\kappa} + \frac{1}{\sigma}\right) a\left\{i_{oS,ref}\left[\exp\left(\frac{\alpha_{aS}F}{RT}(\eta - \Delta U)\right) - \exp\left(-\frac{\alpha_{cS}F}{RT}(\eta - \Delta U)\right)\right]\right.$$

$$\left. - \left(-\frac{nF}{s_R}\right)\frac{\frac{c_R}{c_{Rf}} - \exp\left[(\alpha_{aR} + \alpha_{cR})F\eta/RT\right]}{\frac{1}{c_{Rf}k_m} - \frac{nF}{s_R i_{oR,ref}}\exp\left[\alpha_{cR}F\eta/RT\right]}\right\} . \quad [23]$$

Before equations 22 and 23 can be solved simultaneously for $c_R$ and $\eta$, four boundary conditions are required. For $c_R$ the following conditions were used

$$c_{Rf}v = c_R v - \varepsilon(D_R + D_a)\frac{dc_R}{dx} \quad \text{at} \quad x = 0 \quad [24]$$

where $c_{Rf}$ is the upstream feed concentration, and

$$\frac{dc_R}{dx} = 0 \quad \text{at} \quad x = L \quad [25]$$

-- the Danckwerts,[19] Wehner-Wilhelm[20] conditions when axial diffusion and dispersion are included. The conditions on $\eta$ depend on the

placement of the counterelectrode. For an upstream counterelectrode, the current density is zero in the matrix phase at the cathode inlet and equal to -i (the total current density to the electrode) in the pore solution phase; the opposite is true at the cathode outlet. Application of these conditions to equation 20 yields appropriate conditions on $\eta$ :

$$\frac{d\eta}{dx} = -\frac{i}{\kappa} \quad \text{at} \quad x = 0 \ , \qquad [26]$$

and

$$\frac{d\eta}{dx} = \frac{i}{\sigma} \quad \text{at} \quad x = L \ . \qquad [27]$$

To reduce the large number of parameters, equations 22 through 27 may be expressed in dimensionless form:

Material balance

$$\frac{d\theta}{dy} = D' \frac{d^2\theta}{dy^2} - \frac{\theta - P_1 \exp\left[(\alpha_{aR}/\alpha_{cR} + 1)\eta'\right]}{1 + \exp(\eta')} \ . \qquad [28]$$

Potential distribution

$$\frac{d^2\eta'}{dy^2} = P_2 \left\{ P_3 \exp(-\alpha_{cS}\eta'/\alpha_{cR}) \left[ 1 - P_4 \exp\left( \frac{\alpha_{aS} + \alpha_{cS}}{\alpha_{cR}} \eta' \right) \right] + \frac{\theta - P_1 \exp\left[(\alpha_{aR}/\alpha_{cR} + 1)\eta'\right]}{1 + \exp(\eta')} \right\} \ . \qquad [29]$$

Boundary conditions

$$\theta - D' \frac{d\theta}{dy} = 1 \quad \text{and} \quad \frac{d\eta'}{dy} = P_5 I^* \quad \text{at} \quad y = 0 \ , \qquad [30]$$

and

$$\frac{d\theta}{dy} = 0 \quad \text{and} \quad \frac{d\eta'}{dy} = -P_6 I^* \quad \text{at} \quad y = \alpha L \ , \qquad [31]$$

where $\theta$ is the reactant concentration divided by its value upstream in the feed. Here the distance and the overpotential were made dimensionless in such a manner as to emphasize the pertinent physical phenomena. The dimensionless coordinate $y$, as suggested by the limiting current analysis,[1] is the physical distance $x$ divided by the quantity $1/\alpha = v/a\ k_m$, representing the effective depth of penetration of the reaction into the electrode at the limiting current. In this way, the parameter

$$D' = (D_R + D_a)a\ k_m/v^2 \qquad [32]$$

relates to the effect of axial diffusion and dispersion. For flow-through reactors, effects of convection, reaction, and mass-transfer to the wall are dominant, while axial diffusion and dispersion are secondary. Thus, it is appropriate to have these latter effects included in only one parameter, $D'$, and to have the dimensionless coordinate $y$ determined by the dominant effects. However, at low Péclet numbers, $v/a\ D_o < 100$, axial diffusion and dispersion effects are not small,[14] and the inclusion of the corresponding terms in equation 28 and in the boundary condition (equation 30) is necessary.

The local overpotential $\eta$ was made dimensionless by the relation

$$\exp(\eta') = -\frac{nFk_m c_{Rf}}{s_R i_{oR,ref}} \exp(\alpha_{cR} F\eta/RT) , \qquad [33]$$

which also shifts the overpotential by an additive amount based on the exchange current density $i_{oR,ref}$ of the main reaction and the feed concentration $c_{Rf}$ of the reactant. This shift is in recognition of the fact that the electrode will be run with a relatively high

electric driving force so that the main reaction can be carried to a high degree of completion. The backward term of the main reaction is then characterized by the parameter

$$P_1 = \left( - \frac{s_R i_{oR,ref}}{nFk_m c_{Rf}} \right)^{1+\alpha_{aR}/\alpha_{cR}} , \qquad [34]$$

which will be insignificant when the reaction exhibits Tafel behavior.

Under these conditions, the relative importance of the ohmic potential drop within the porous electrode is characterized by the parameter

$$P_2 = \frac{\alpha_{cR} nF^2 v^2 c_{Rf}}{s_R a\, k_m RT} \left( \frac{1}{\kappa} + \frac{1}{\sigma} \right) , \qquad [35]$$

and the side reaction is characterized by

$$P_3 = - \frac{s_R i_{oS,ref}}{nF\, k_m c_{Rf}} e^{\alpha_{cS} F\Delta U/RT} \left( - \frac{nF\, k_m c_{Rf}}{s_R i_{oR,ref}} \right)^{\alpha_{cS}/\alpha_{cR}} \qquad [36]$$

at the half-wave potential of the main reaction. The half-wave potential may be calculated from equation 33 by setting $\eta'$ equal to zero. This is seen from the second term on the right side of equation 28, which represents the dimensionless transfer current of the primary reaction -- setting $\eta'$ equal to zero yields a value in the denominator of two. The backward term of the side reaction is

characterized by the magnitude of the parameter

$$P_4 = \left( - \frac{s_R i_{oR,ref}}{nF\, k_m c_{Rf}} \right)^{\frac{\alpha_{aS}+\alpha_{cS}}{\alpha_{cR}}} \exp\left[-F(\alpha_{aS} + \alpha_{cS})\Delta U/RT\right] . \quad [37]$$

The parameters $P_5$ and $P_6$ represent the relative importance of the ohmic potential drop in the pore solution phase and the matrix phase, respectively, and are related to the parameter $P_2$ :

$$P_5 = - \frac{\sigma P_2}{\sigma + \kappa} , \quad [38]$$

and

$$P_6 = - \frac{\kappa P_2}{\sigma + \kappa} , \quad [39]$$

so that

$$-P_2 = P_5 + P_6 . \quad [40]$$

The total current density $i$ to the reactor was made dimensionless with the limiting current density that would exist if all the reactant in the feed were completely reacted:

$$I^* = \frac{s_R i}{nFvc_{Rf}} . \quad [41]$$

## Numerical Solution

The governing equations 28 and 29 were first linearized about a trial solution and then, along with the boundary conditions (equations 30

and 31), cast in finite-difference form accurate to order $h^2$, where h is the dimensionless distance between the mesh points, and solved by a numerical technique developed by Newman.[23]

Unfortunately, it was found that the standard central-difference approximations of the derivatives were not sufficiently accurate to approach the limiting-current result, which can be calculated analytically. This anomalous behavior was primarily due to the high degree of non-uniformity in the current and concentration distributions near the front of the electrode. Therefore, to obtain accurate results, new finite-difference approximations to the derivatives were developed (see Appendix).

## Results

Comparisons between model predictions and experiments. For the calculations to be presented, the counterelectrode is upstream, the primary reaction is the deposition of copper, and the side reaction is the generation of dissolved hydrogen. Two types of data on copper removal[1,13] are utilized to demonstrate the effectiveness of the model. In the first data set,[1] predictions of the overall reactor performance are tested -- this includes predicting the current-potential behavior of the porous cathode and the effluent concentration of the reactant species. The remaining data set[13] is used to test model calculations of the current distribution within the porous cathode.

Figure 1 displays the model fit to the data of Bennion and Newman[1] for copper removal using a porous carbon electrode. The quantities I

and VOP are the total current to the reactor and the potential of the cathode current collector relative to a saturated calomel reference electrode placed in the effluent stream, respectively. The experimental effluent copper concentrations (in mg/ℓ) are shown as the numbers

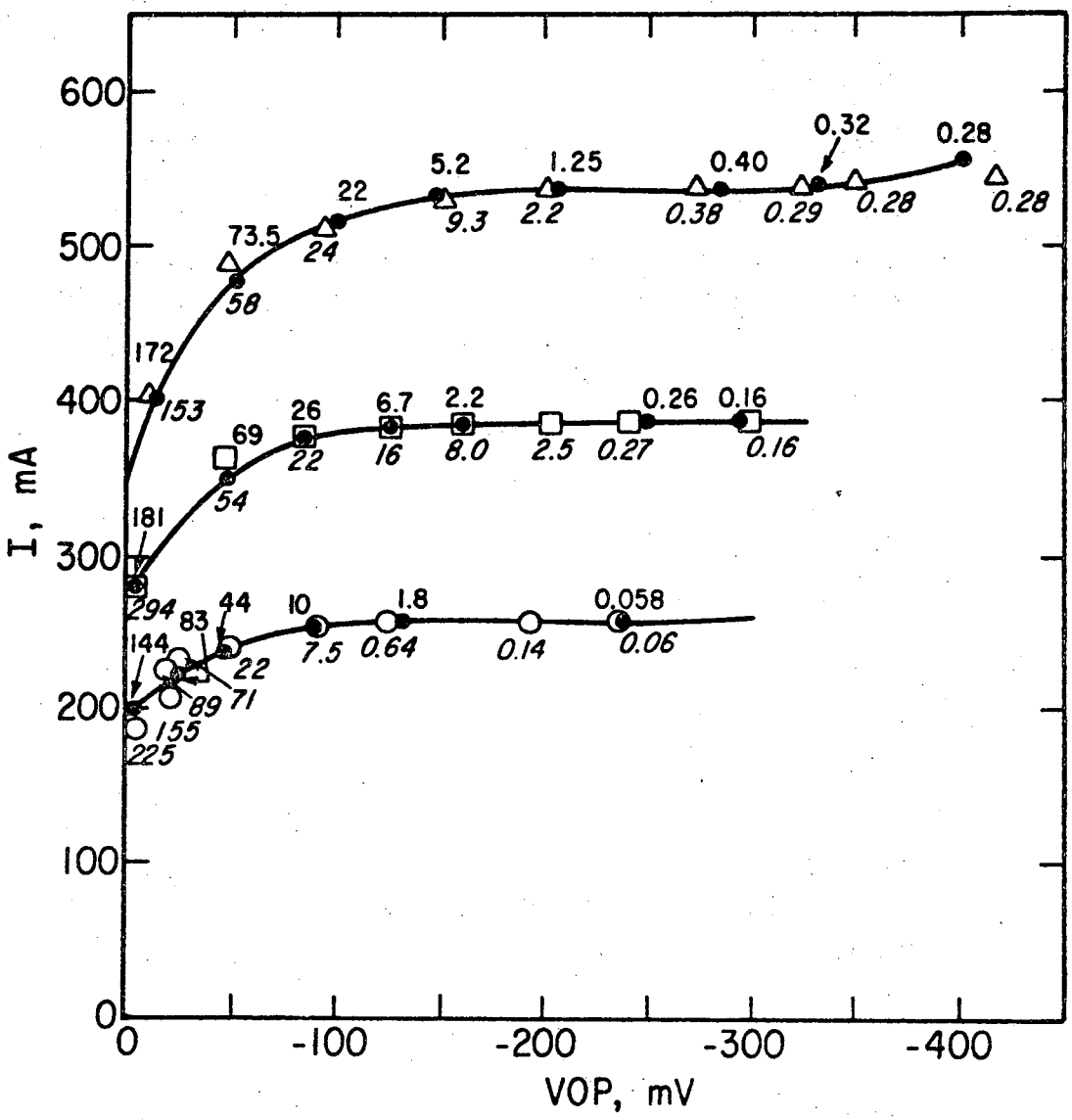


XBL 7611-9795

Figure 1. Current-potential curves for an electrode 10.1 cm in diameter and 6 cm deep,[1] packed with porous carbon flakes and chips. Open symbols are experimental data points; closed symbols are calculated. Calculated effluent concentrations (in mg/ℓ) are indicated above the corresponding points in upright type; experimental values are given in italic type below the corresponding data points. The flow rate was 8 $cm^3$/min for the circles, 12 $cm^3$/min for the squares, and 16 $cm^3$/min for the triangles.

below each curve corresponding to the open triangles Δ, squares □, and circles O. The numbers above each curve correspond to the solid circles ● and are the calculated values of the effluent copper concentration. Values of the parameters used to fit the data shown in Figure 1 are given in Table 1.

Five parameters were adjusted to obtain agreement between the calculated and experimental values in Figure 1: one value of the exchange current density for copper deposition was determined by fitting the data at the left side of the top curve; one value of the exchange current density for hydrogen evolution attempts to fit the rise in the current due to the observed onset of hydrogen evolution at the right side of the top curve; and three values of the mass-transfer coefficient $k_m$ corresponding to the three different flow rates were determined mainly by the effluent concentration at the right side of each experimental curve.

In Figure 2, the fitted values of $k_m$ (shown by the open triangles Δ) have been plotted in terms of the dimensionless Sherwood number $\varepsilon k_m/aD_o$ as a function of the dimensionless Péclet number $v/aD_o$. The upper dashed line is the Wilson and Geankoplis correlation[24]

$$\frac{\varepsilon k_m}{aD_o} = \frac{1.09}{[6(1-\varepsilon)]^{2/3}} \left(\frac{v}{aD_o}\right)^{1/3} , \qquad [42]$$

and the lower dashed line is a correlation suggested by Bird et al.[25]

$$\frac{\varepsilon k_m}{aD_o} = 0.91\ \varepsilon \left(\frac{v}{a\nu\psi}\right)^{0.49} \psi^2 \left(\frac{\nu}{D_o}\right)^{1/3} , \qquad [43]$$

Table 1. Values of the parameters used in fitting the data in Figure 1 and in generating the curves in Figures 5 through 11.

| | | |
|---|---|---|
| $a = 25\ cm^{-1}$ | $\varepsilon = 0.3$ | $D_o = 6\times10^{-6}\ cm^2/s$ |
| $\kappa_o = 0.17$ mho/cm | $\sigma = 10^4$ mho/cm | $s_R = -1$ |
| $n = 2$ | $T = 298.15$ K | $\alpha_{aR} = 1.5$ |
| $\alpha_{cR} = 0.5$ | $\gamma = 0.75$ | $\alpha_{aS} = 0.5$ |
| $\alpha_{cS} = 0.5$ | $U_S-U_R = 0.281$ V | $L = 6$ cm |

| $k_m\times10^4$, cm/s | $v\times10^3$, cm/s |
|---|---|
| 1.922 | 3.328 |
| 1.620 | 2.496 |
| 1.315 | 1.664 |

$i_{oR} = 3.8\times10^{-5}\ A/cm^2$ at $c_R = 0.1$ mole/ℓ

$i_{oS} = 7\times10^{-6}\ A/cm^2$ at $c_S = 1$ mole/ℓ, $p_S = 1$ atm

$i_{oS,ref} = 3.717\times10^{-12}\ A/cm^2$

dimensionless parameters as a function of $c_{Rf}$ and v

| $c_{Rf}\times10^5$, moles/cm$^3$ | 1.050 | 1.050 | 1.050 | 1.011 | 1.003 | 0.1003 | 0.01003 |
|---|---|---|---|---|---|---|---|
| $v\times10^3$, cm/s | 9.984 | 6.656 | 3.328 | 2.496 | 1.664 | 1.664 | 1.664 |
| $P_1\times10^9$ | 9.461 | 22.99 | 104.9 | 215.9 | 501.3 | 5013. | 50130. |
| $P_2$ | -16.05 | -8.905 | -3.254 | -2.091 | -1.136 | -0.1136 | -0.01136 |
| $P_3\times10^5$ | 1.247 | 1.247 | 1.247 | 1.295 | 1.305 | 13.05 | 130.5 |
| $P_4\times10^9$ | 1.761 | 2.745 | 5.863 | 8.253 | 12.53 | 12.53 | 12.53 |
| $P_5$ | 16.05 | 8.905 | 3.254 | 2.091 | 1.136 | 0.1136 | 0.01136 |
| $P_6\times10^6$ | 44.83 | 24.87 | 9.089 | 5.842 | 3.173 | 0.3173 | 0.03173 |
| $D'\times10^2$ | 7.385 | 8.877 | 12.17 | 13.68 | 16.70 | 16.70 | 16.70 |

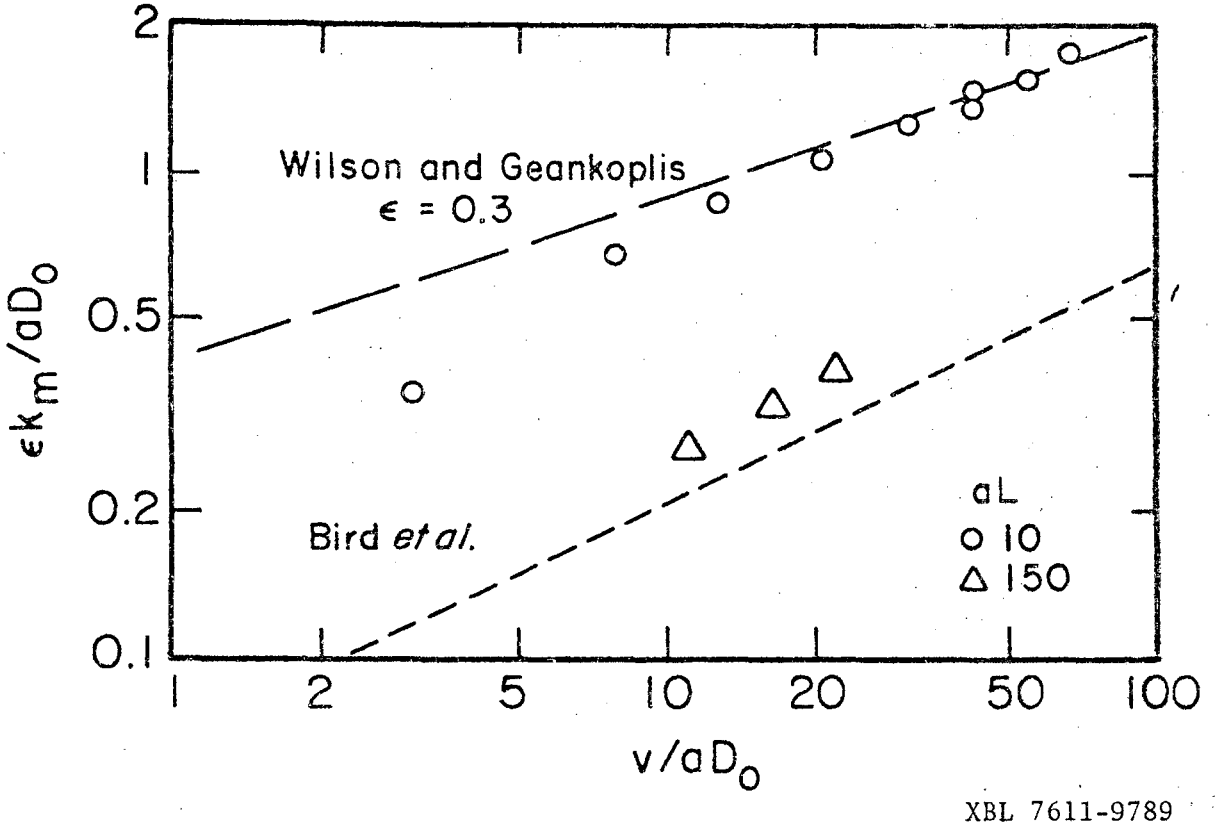


Figure 2. Correlation of the Sherwood number as a function of Péclet number and dimensionless electrode thickness aL. Open triangles come from a fit of the data of figure 1; open circles are the results of Appel and Newman.[26] Two correlations from the literature are also shown.

where a value of $\varepsilon = 0.3$ has been used in calculating each line. Also shown in Figure 2 by means of the open circles O are the data of Appel and Newman[26] where $\varepsilon = 0.372$ . It should be noted that it has been assumed that the dimensionless correlations for $k_m$ (given by equation 42 and 43) have been corrected for dispersion; Appel's results have not, and therefore $k_m$ in this case is fundamentally a different quantity (see reference 14 for this correction and a discussion of different definitions of $k_m$ ).

The model fit of the limiting current-distribution data of Alkire and Gracon[13] for copper deposition on platinum screen electrodes is shown in Figure 3. The transfer current density for the main reaction $di_{2R}/dx$ has been normalized by the total current density $i_R$ due to the primary reaction and the electrode length $L$ . A uniform current distribution would correspond to a horizontal line at an ordinate value of 1. Values of the parameters used to fit these data are given in Table 2.

The data for the smallest flowrate (v = 0.1067 cm/s) were fitted first by using literature values of the exchange current densities for copper deposition and hydrogen evolution on copper[23,27] (any $i_o$ values would work, however, since the data[13] were obtained at the limiting current) and adjusting the value of the mass-transfer coefficient $k_m$ to obtain reasonable agreement between the calculated and experimental values. This value for the mass-transfer coefficient was then used to change the coefficient in the Wilson-Geankoplis correlation[24] (given by equation 42) to 0.85:

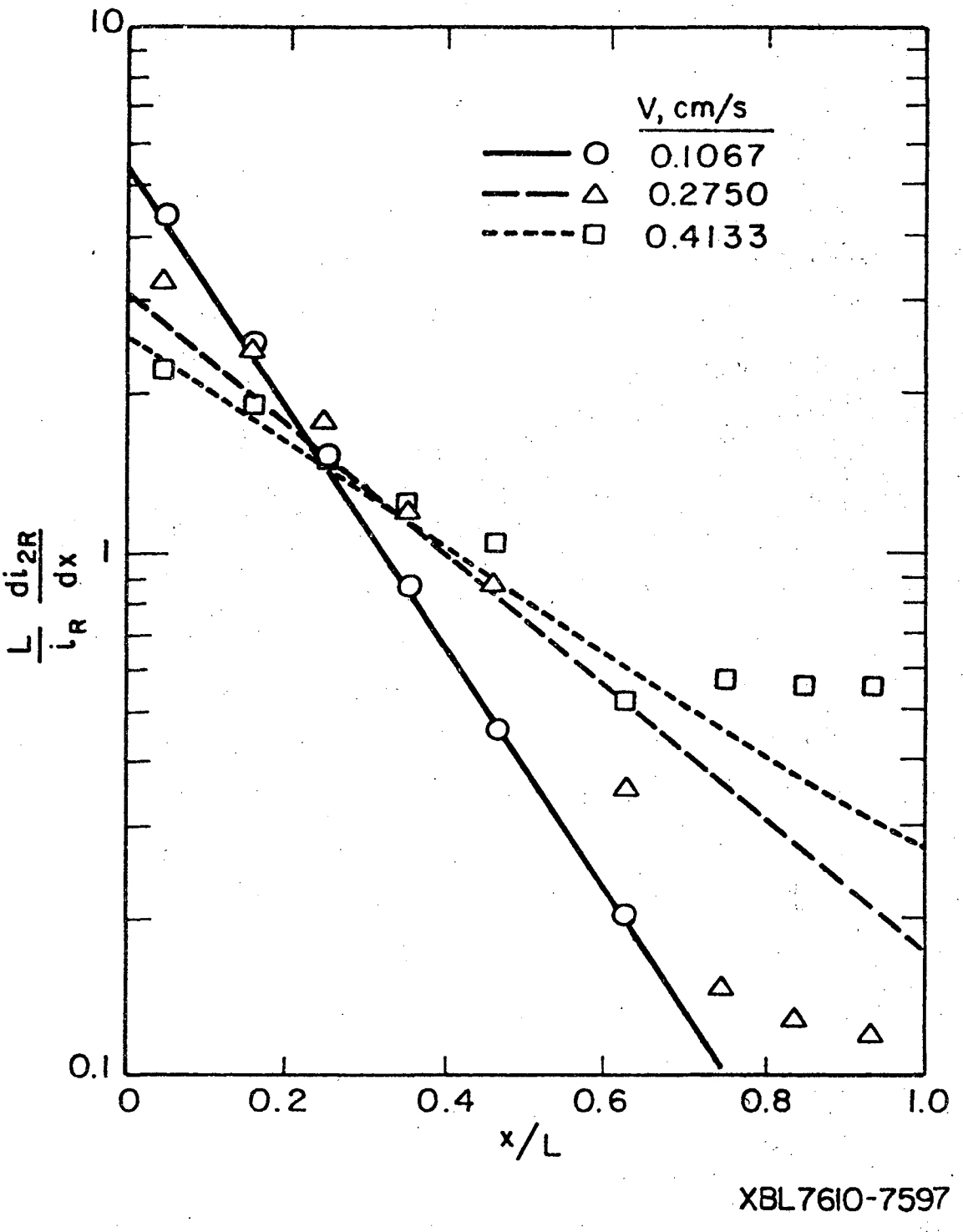


Figure 3. Normalized distribution of copper deposition. Experimental data[13] and calculations are for deposition from a 2 mM cupric solution onto a bed 0.4 cm thick with a porosity of 0.64 and a specific surface area of 260 $cm^{-1}$, constructed of layers of Pt screens.

Table 2. Values of the parameters used in fitting the data in Figure 3.

| | | |
|---|---|---|
| $a = 260\ cm^{-1}$ | $\varepsilon = 0.64$ | $D_o = 7.6\times10^{-6}\ cm^2/s$ |
| $\kappa_o = 0.55$ mho/cm | $\sigma = 10^4$ mho/cm | $s_R = -1$ |
| $n = 2$ | $T = 298.15$ K | $\alpha_{aR} = 1.5$ |
| $\alpha_{cR} = 0.5$ | $\gamma = 0.75$ | $\alpha_{aS} = 0.5$ |
| $\alpha_{cS} = 0.5$ | $U_S-U_R = 0.481$ V | $L = 0.4$ cm |

$i_{oR} = 10^{-3}\ A/cm^2$ at $c_R = 0.1$ mole/ℓ

$i_{oS} = 10^{-7}\ A/cm^2$ at $c_S = 1$ mole/ℓ, $p_S = 1$ atm

$i_{oS,ref} = 1.732\ 10^{-12}\ A/cm^2$

dimensionless parameters

as a function of v

($c_{Rf} = 2\times10^{-6}$ mole/cm$^3$)

| v, cm/s | 0.1067 | 0.2750 | 0.4133 |
|---|---|---|---|
| $P_1\times10^9$ | 290.3 | 82.17 | 47.73 |
| $P_2$ | -0.1968 | -0.9532 | -1.880 |
| $P_3\times10^5$ | 3.779 | 3.779 | 3.779 |
| $P_4\times10^{12}$ | 4.001 | 2.128 | 1.622 |
| $P_5$ | 0.1967 | 0.9532 | 1.880 |
| $P_6\times10^6$ | 5.540 | 26.84 | 52.93 |
| $D'\ 10^2$ | 6.040 | 3.203 | 2.439 |

$$\frac{\varepsilon k_m}{aD_o} = \frac{0.85}{[6(1 - \varepsilon)]^{2/3}} \left(\frac{v}{aD_o}\right)^{1/3} . \qquad [44]$$

The remaining lines in Figure 3 for the higher flowrates were then calculated using this expression for the mass-transfer coefficient and no additional adjustment of parameters.

It may be noted that Alkire and Gracon[13] proposed that the estimated specific interfacial area be reduced by a multiplier of 0.81 to yield an adjusted value. When used in the Wilson-Geankoplis correlation,[24] this effectively reduces the coefficient to 0.947 if one continues to use the estimated value. In this case, the value of $ak_m$ (which is the quantity which enters into the model equations) is reduced by a multiplier of 0.704 from the value which would be predicted by the Wilson-Geankoplis correlation and the estimated area. By our reducing the coefficient from 1.09 to 0.85, we have effectively reduced the value of $ak_m$ by a multiplier of 0.78. Alkire and Gracon's choice of the multiplier of 0.81 was evidently based on the values of the total limiting current, not on a fit of the distribution data as in Figure 3.

Theoretical predictions. -- Again the results presented are divided into two categories, microscopic distributions and overall reactor performance. For the calculations which follow, the counter-electrode is upstream, the primary reaction is again the deposition of copper, and the side reaction is the generation of dissolved hydrogen.

Figure 4 shows the reaction rate distributions for the primary electrode reaction only, at and below the limiting current, for the

physical parameters and dimensionless parameters (corresponding to $v = 3.328\times10^{-3}$ cm/s) in Table 1, but with $P_3$ and $P_4$ equal to zero (i.e., a single electrode reaction). The limiting current distribution includes the effect of axial diffusion and dispersion and was determined from the analysis of Newman and Tiedemann:[14]

$$\frac{di_2^*}{dy} = \frac{Be^{-y/B} + (B - 1)e^{By/D'} \exp\left[-\alpha L\left(\frac{1}{B} + \frac{B}{D'}\right)\right]}{B^2 - \frac{D'}{B}(B - 1)\exp\left[-\alpha L\left(\frac{1}{B} + \frac{B}{D'}\right)\right]} \qquad [45]$$

where

$$i_2^* = \frac{s_R i_2}{nFvc_{Rf}}, \qquad [46]$$

and

$$B = \frac{1 + \sqrt{1 + 4D'}}{2}. \qquad [47]$$

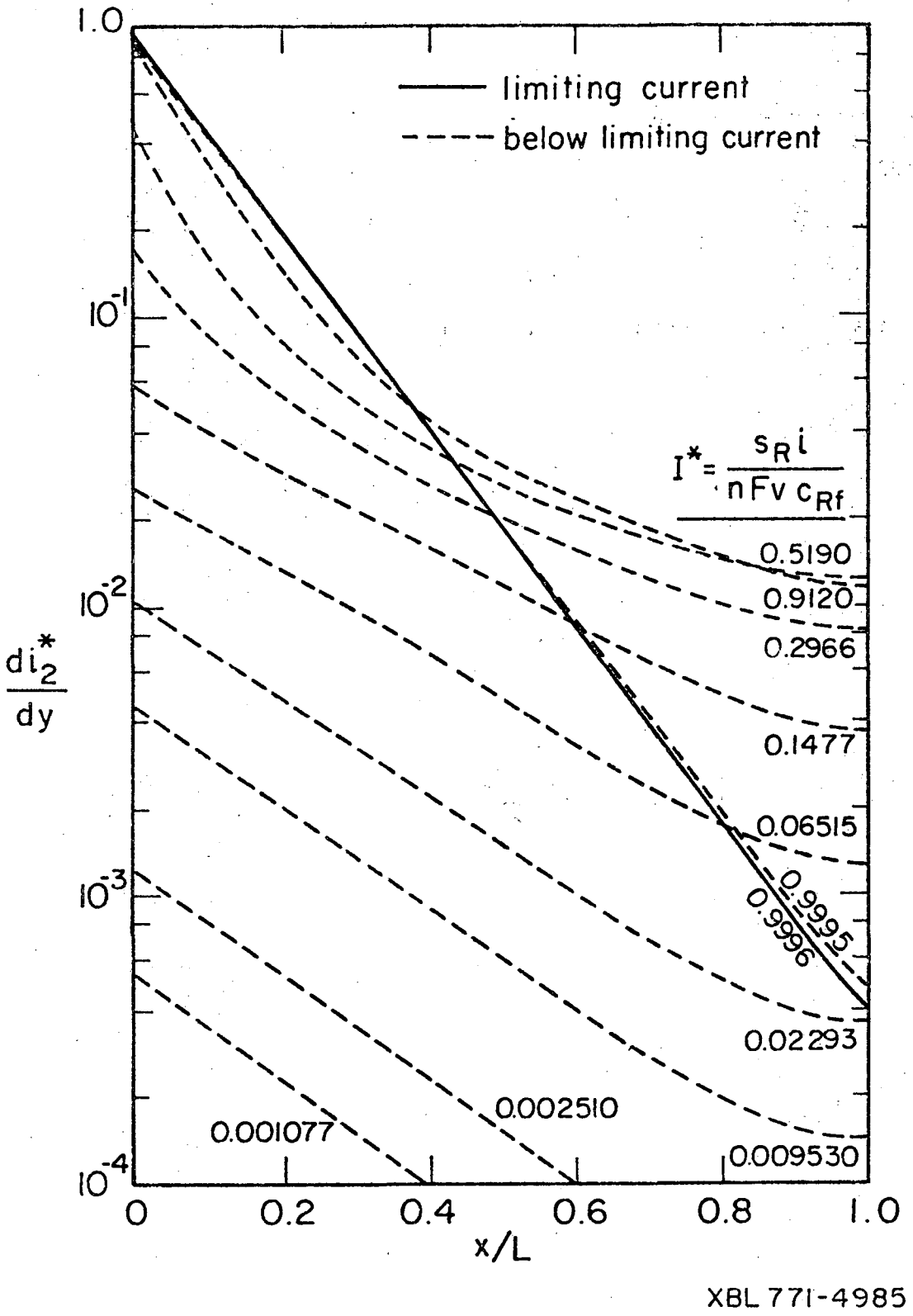


Figure 4. Reaction distribution for copper deposition in the absence of a side reaction, calculated for $\alpha L = 8.663$, $D' = 0.1217$, and $P_2 = -3.254$.

Integration of equation 45 from $y = 0$ to $y = \alpha L$ yields an expression for the total dimensionless limiting current density to the electrode:

$$-i_2^*(0) = I^* = \frac{1 - e^{-\alpha L/B} + \frac{D'(B-1)}{B^3} \exp\left[-\alpha L \frac{1}{B} + \frac{B}{D'}\right] (e^{B\alpha L/D'} - 1)}{1 - \frac{D'}{B^3}(B - 1) \exp\left[-\alpha L \frac{1}{B} + \frac{B}{D'}\right]} . \qquad [48]$$

Figures 5 through 8 show current, potential, current efficiency, and concentration distributions within a reactor operating at conditions which correspond to the point on the upper curve of Figure 1 where VOP = -403 mV and the outlet concentration is 0.28 mg/ℓ .

In Figure 9 the solution-phase ohmic potential drop $\Delta\Phi_2$ across a reactor has been plotted as a function of the electrical driving force at the back of the reactor $(\Phi_1 - \Phi_2)_{\alpha L}$ for two cases: 1) the primary reaction only and 2) when the side reaction is included, for values of the physical parameters and dimensionless parameters (corresponding to $v = 3.328\times10^{-3}$ cm/s) in Table 1. The ohmic potential drop has been made dimensionless with the quantity

$$\Delta\Phi_2' = \frac{nFvc_{Rf}}{s_R\kappa} \frac{v}{ak_m} , \qquad [49]$$

which is an estimate of the ohmic potential drop across a reactor operating at the limiting current[1] when the effluent concentration is zero and the effects of axial diffusion and dispersion are negligible.

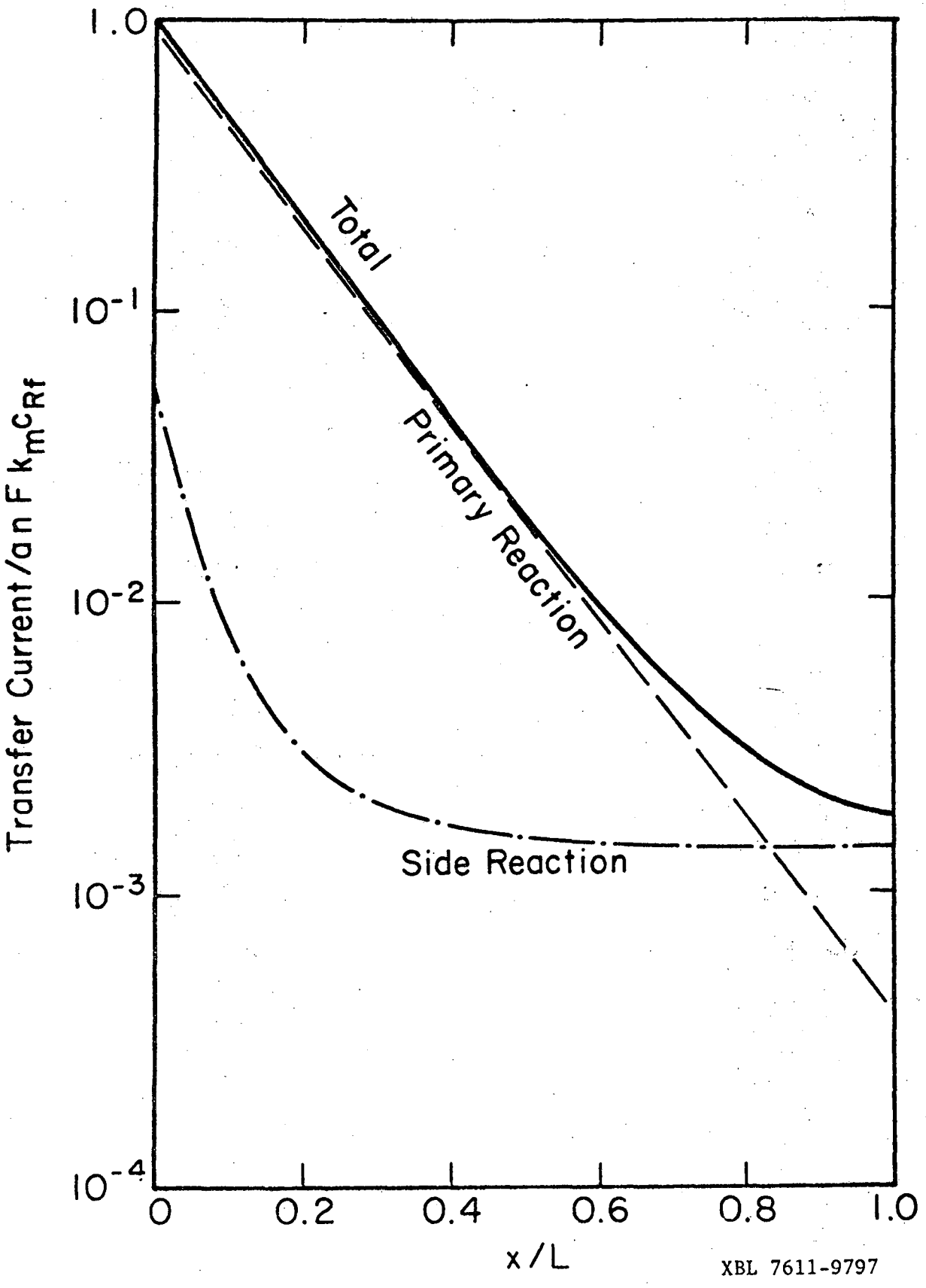


Figure 5. Current distributions for deposition of copper and generation of dissolved hydrogen within a porous electrode with fluid flow from left to right, calculated for v = 0.003328 cm/sec, $a = 25\ cm^{-1}$, $\varepsilon = 0.3$, L = 6 cm, $c_{Rf} = 0.0105$ mole/ℓ, and VOP = -0.403 V relative to a calomel reference electrode in the dilute-product stream.

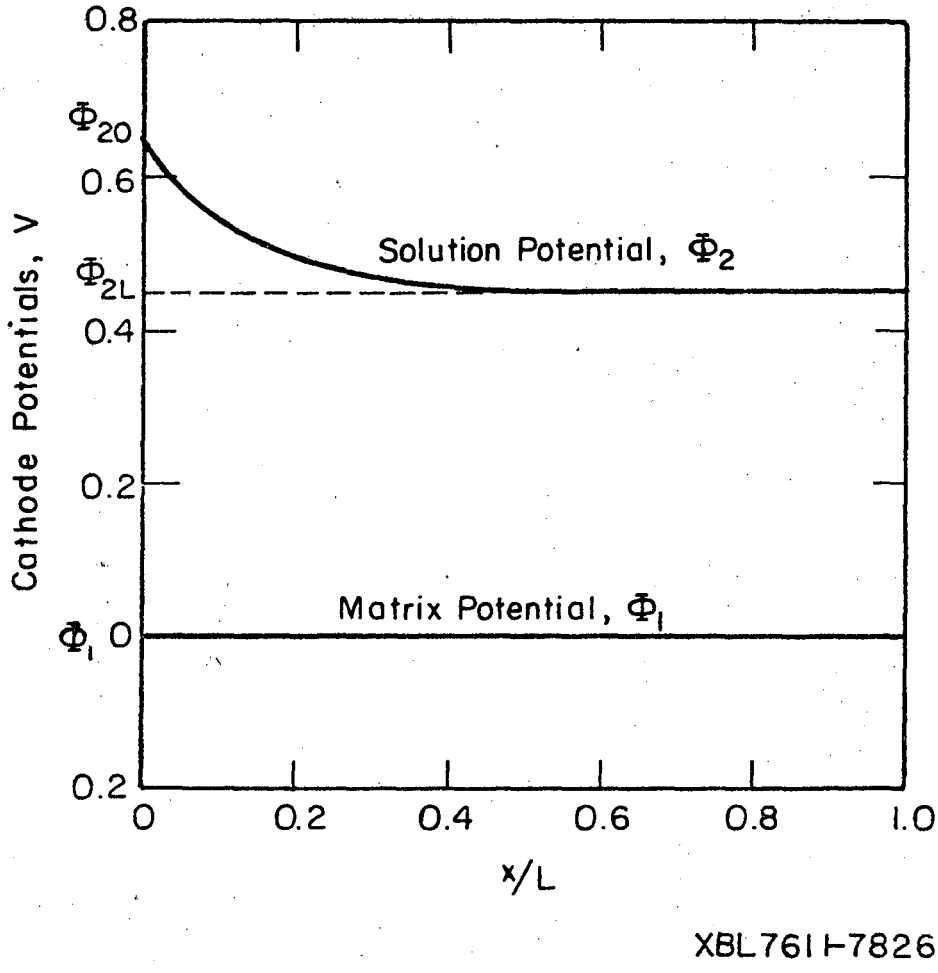


Figure 6. Solution-phase and solid-matrix-phase potentials, as functions of cathode position, for the conditions of Figure 5.

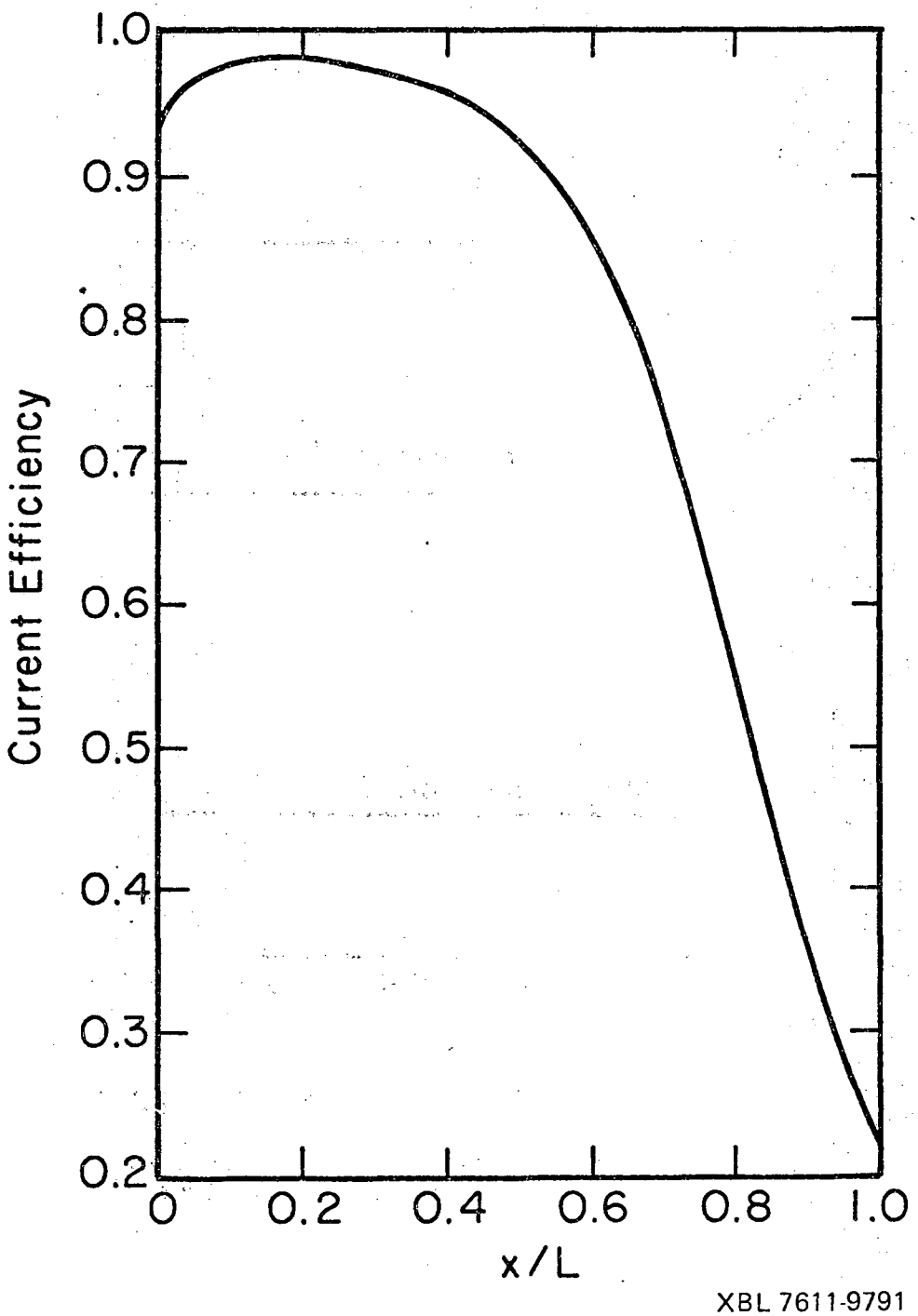


Figure 7. Local current efficiency as a function of cathode position, for the conditions of Figure 5. The overall current efficiency is 0.962.

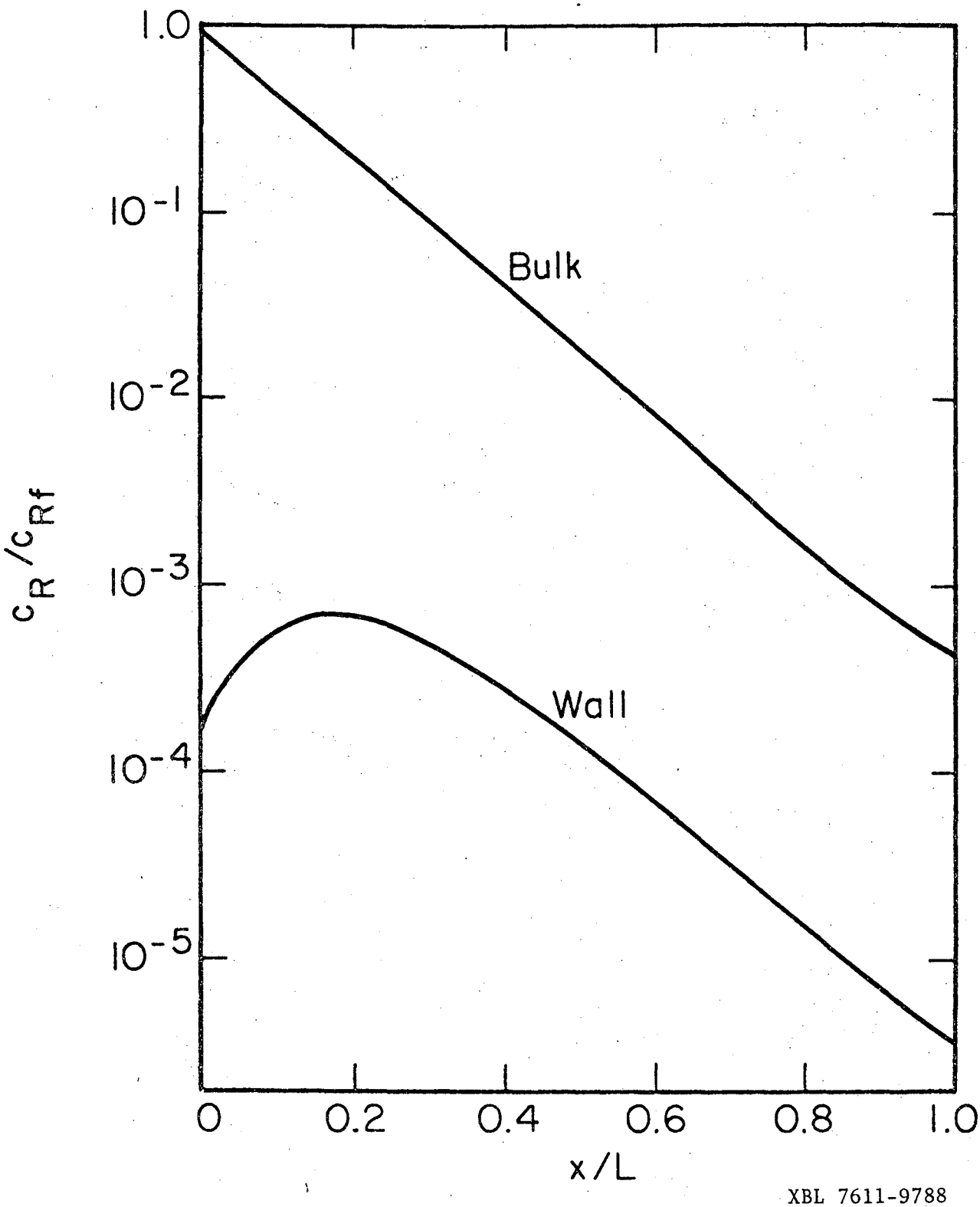


Figure 8. Distribution of copper concentration in the flowing stream and along the pore wall, for the conditions of figure 5.

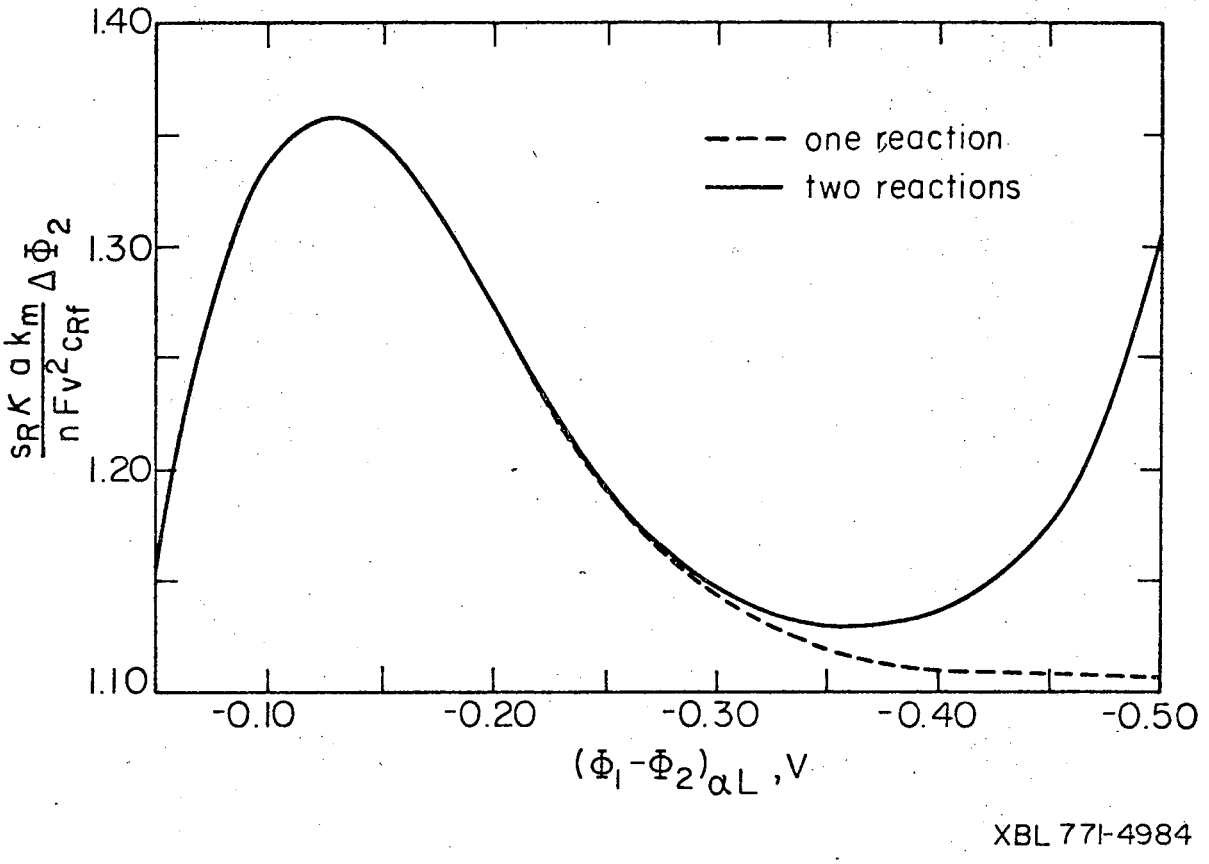


Figure 9. Ohmic potential drop across the solution within the porous electrode -- under the conditions of figure 4 and also with simultaneous generation of dissolved hydrogen.

The potential $(\Phi_1 - \Phi_2)_{\alpha L}$ is the potential of the cathode current collector relative to a copper reference electrode (with a concentration of $c_{Rf}$ in the reference electrode compartment) placed at the back of the reactor.

At large negative values of $(\Phi_1 - \Phi_2)_{\alpha L}$ when only the primary reaction is considered, the ordinate approaches the value predicted by the limiting-current analysis of Newman and Tiedemann:[14]

$$\frac{\Delta\Phi_2}{\Delta\Phi_2'} = \frac{\left(1 + \frac{D'}{B^2}\right)\left[B^2 - (\alpha L + 1 + D')e^{-\alpha L/B}\right]}{B + \frac{D'}{B^2}(1 - B)\exp\left[-\alpha L\,\frac{1}{B} + \frac{B}{D'}\right]} - \frac{D'}{B}, \qquad [50]$$

and has a value of 1.1057 in this case.

Figures 10 and 11 show the effect on the current-potential curve if the fluid velocity is increased or the feed concentration decreased. The curve labeled with a v in Figure 10 corresponds to the upper curve in Figure 1, and the curve labeled $10^{-2}$M in Figure 11 corresponds to the lower curve in Figure 1. (See also Table 1.)

## Discussion

Agreement between model calculations and the experimental data of Bennion and Newman[1] shown in Figure 1 should be considered satisfactory. However, the values of the parameters found by fitting the data need some clarification.

The fitted values of the exchange current densities for copper deposition and hydrogen evolution on carbon (see Table 1) are 0.035

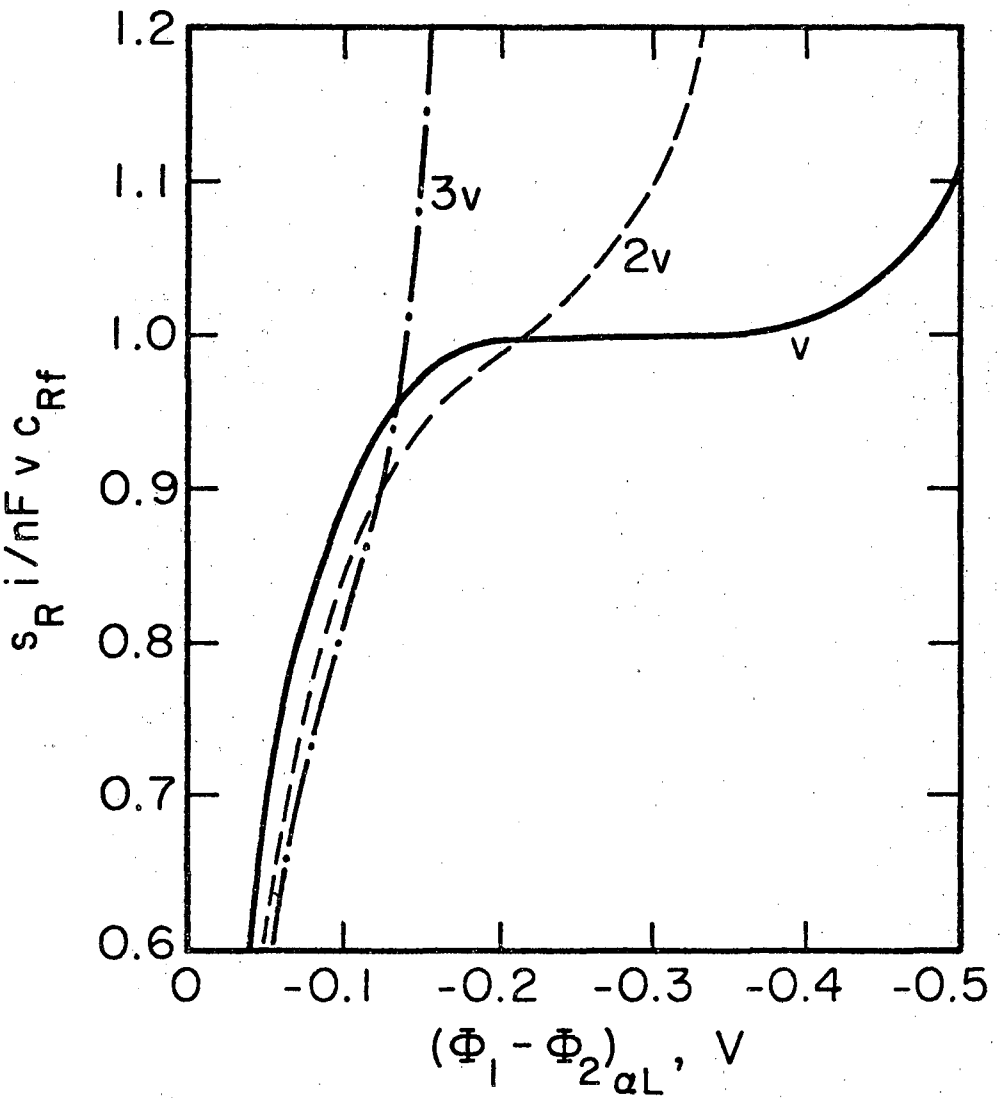


Figure 10. Effect of flow rate on the current-potential curve. Operation at flow rates substantially above the design value[1] (here v = 0.003328 cm/s) obscures the limiting-current plateau because of the high ohmic potential drop in the solution phase. For parameter values, see Table 1.

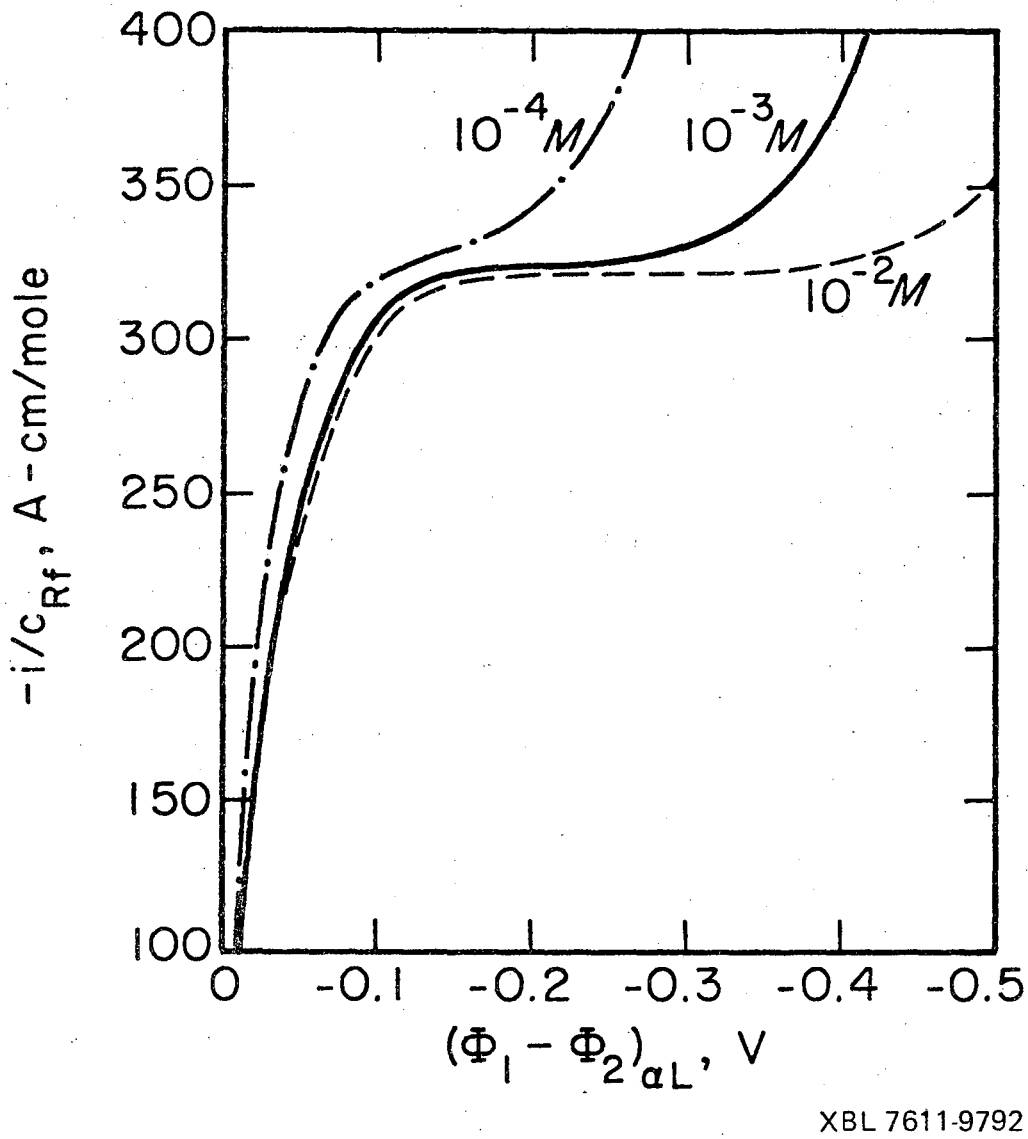


Figure 11. Effect of feed concentration on the current-potential curve. Low concentrations correspond to low currents for the primary reaction, and these are easily obscured by the side reaction even in the absence of a significant ohmic potential drop within the reactor. For parameter values, see Table 1.

and 70 times the reported literature values ($i_{o,Cu} = 10^{-3}$ A/cm$^2$ [23] and $i_{o,H_2} = 10^{-7}$ A/cm$^2$ [27]) for these reactions on copper, respectively. However, it should not be interpreted that there is anything fundamental about these fitted values since the data are insufficient at the extreme values of the current to provide for their accurate evaluation. We also wish to emphasize that we do not suggest this as a method for determining fundamental kinetic parameters, since the bed is operating with a highly nonuniform current density and mass-transport limitations dominate the data in certain regions.

The fitted values of $k_m$ (given in Table 1), determined mainly by the effluent concentration at the right on the experimental curves of Figure 1 and plotted in Figure 2, show a clear dependence on the velocity as follows

$$\frac{\varepsilon k_m}{aD_o} = 0.07054 \left(\frac{v}{aD_o}\right)^{0.5454} . \qquad [51]$$

Data obtained in this manner[1] yields fundamental information about $k_m$ (e.g. Appel and Newman[26]). Unfortunately, the value used for the specific interfacial area $a$ of 25 cm$^{-1}$ is an effective value and may be low by a factor of 4 to 12.[28] If larger values of $a$ are used, the value of $k_m$ will decrease, and the triangles plotted in Figure 2 would move down and to the left toward lower values of the Sherwood and Péclet numbers.

The purpose of Figure 2 is to call attention to the fact that the behavior of $k_m$ is not well established in this flow region.

Newman and Tiedemann[14] have suggested, for a restricted range of flow rates: $1 \leq Pe < 10^4$ and $Re < 10$, where $Pe$ is the Péclet number $v/aD_o$ and $Re$ is the Reynolds number $v/a\nu$, there should exist an entry region such that the local mass-transfer coefficient is larger than the asymptotic value for deep bed electrodes and that the average value of the mass-transfer coefficient will be dependent on the quantity $aL$.

Since most measurements for $k_m$ involve short electrodes, small $aL$ (e.g. equation 42 of Wilson and Geankoplis,[24] where $1.8 \leq aL \leq 27$), the entire electrode may be within the entry region and will therefore predict too large a value for $k_m$ when $aL$ is large (deep beds) as is the case for Bennion and Newman's data.[1]

Also in Figure 2, a correlation found in Bird et al.[25] (equation 43) has been extrapolated by at least an order of magnitude in Reynolds number below the range for which the correlation has been tested. However, this equation appears to give a conservative estimate for $k_m$ and may be useful for design purposes until better correlations are developed for this region of flow.

In Figure 3 agreement between model calculations and the experimental data of Alkire and Gracon[13] for the smallest flow rate (0.1067 cm/s) is good. The almost linear behavior on the semi-log plot for the predicted limiting current distribution is expected based on the analysis of Bennion and Newman[1] for the special case of mass-transfer control. As expected, the value of $k_m$ which best fits the data (given by equation 44) is less than that predicted

by equation 42 of Wilson and Geankoplis[24] due to the large value of $aL = 104$. The reason for using equation 44 at the two higher flowrates is to have some basis for changing $k_m$ with the velocity since no data on the effluent concentration are given in reference 13 to enable an estimation of $k_m$ as was done with the data of Bennion and Newman[1] in Figure 1. (A graph of the total limiting current is presented by Alkire and Gracon[13], from which one could infer the effluent concentration if side reactions are negligible. However, values from this graph cannot be obtained with great precision, and, as pointed out by Appel and Newman,[26] the total current is an inherently inaccurate method of measuring the mass-transfer coefficient when the overall conversion is close to 100 percent.)

In Figure 3, at least two reasons are responsible for the discrepancies between the model calculations and the experimental data at the higher flow rates. First the data are a re-plot of data taken from an arithmetic plot and are subject to error. Second $k_m$ may not be a constant throughout the electrode as assumed in the model. However, the discrepancies in Figure 3 are considerably less than those between Alkire and Gracon's Figures 6 and 9, where the lack of explanation has already been noted in the literature.[18] One may speculate as to why the agreement between the model of Alkire and Gracon and their data is poor. This is perhaps due to the inadequate representation of the derivatives in the governing equations at the limiting current by standard central-difference approximations. New finite-difference approximations to the derivatives (developed in the Appendix) are required as discussed earlier.

The reaction rate distribution when only the metal deposition reaction is considered is plotted in Figure 4 for various fractions of the limiting current. The effect of axial diffusion and dispersion is apparent in the limiting current distribution as $di_2^*/dy$ is less than one at $x/L$ equal to zero. The fact that $I^*$ is not equal to one for the limiting current distribution is because mass-transfer limitations exist within the electrode and therefore a small fraction of the feed concentration will escape unreacted.

For an appreciable fraction of the limiting current $(I^* > 0.9)$, the reaction rate near the front of the electrode is high and decreases almost exponentially, similar to the behavior of the limiting current distribution (see equation 45). Near the back of the electrode, the rate of reaction for the limiting current distribution is small because most of the copper is removed near the front of the electrode.

Therefore, the reaction rates below the limiting current are greater at the back of the electrode (for values of $I^* > 0.03$) and are more uniform than the limiting current distribution. Actually, the reaction rate at the back of the electrode $\left(di_2^*/dy|_{y=\alpha L}\right)$ increases as the value of $I^*$ decreases from 0.9996 to 0.7273, passes through a maximum at $I^* = 0.7273$, and then decreases monotonically with $I^*$. Thus the effective depth of penetration of the reaction into the electrode also has a maximum near $I^* = 0.7273$.

For small values of the current $(I^* < 0.03)$, the reaction rate distributions take on the same shape and can be described by a model with linear electrode kinetics and no concentration variations (see Euler and Nonenmacher[29] and Newman and Tobias[30]).

Figure 5 shows the relative rates of reaction for the primary reaction and the side reaction as they are distributed throughout the porous electrode. The total current density to the electrode was chosen close to the limiting current $(I^* = 1.038)$ for the deposition of copper. Consequently, the reaction rate for the primary reaction decreases almost exponentially with distance (see equation 45), as the solution is depleted with copper while flowing through the electrode. The side reaction, generation of dissolved hydrogen, responds mainly to the electric driving force between the solid matrix and the electrolytic solution. Its rate is high near the entrance to the porous electrode and drops to a nearly constant value near the rear. The reason for this can be seen in Figure 6, which represents the variation in the solution-phase potential $\Phi_2$ for a counterelectrode placed upstream of the working electrode.

The matrix conductivity is high, and therefore its potential $\Phi_1$ is nearly a constant. The solution potential $\Phi_2$ varies little near the rear because the current carried in the solution is small in this region. Because the driving force $(\Phi_1 - \Phi_2)$ is essentially uniform for some distance at the back of the electrode, measurement of $(\Phi_1 - \Phi_2)_{\alpha L}$ can lead to a lower bound thermodynamic estimate of the minimum concentration attainable in a flow-through porous electrode (see Trainham and Newman[31] for details).

In Figure 7, the local current efficiency actually goes through a slight maximum near $x/L = 0.18$. The current efficiency is low at the entrance because the high electric driving force leads to a relatively high rate for the side reaction. For somewhat larger values of $x$, the rate of the side reaction decreases more rapidly than the primary reaction, and the local current efficiency rises. However, the primary reaction rate continues to decrease with distance because of the depletion of copper ions, and consequently the local current efficiency eventually drops to about 23 percent at the rear of the electrode. One might well ask, "Why not eliminate the last 40 percent of the thickness of the electrode?"

Figure 8 shows the concentration of copper ions through the thickness of the electrode. The high electric driving force at the entrance results in a very low wall concentration there. As the electric driving force decreases with $x$, the wall concentration rises toward the bulk value. With the diminishing reaction rate through the next part of the electrode, the wall concentration is

able to decrease also, despite the smaller electric driving force in this region. We can also see from this figure that the bulk concentration is depleted by an additional factor of 20 in the last 40 percent of the electrode, despite the lowered current efficiency in this region. This additional metal ion removal can be achieved with relatively little additional expense for the added electrode thickness and virtually no added cost due to added ohmic potential drop.

In Figure 9, the ohmic potential drop across the solution within the reactor exhibits a maximum and then a minimum as the driving force increases at the back of the reactor. The maximum occurs at $I^* = 0.95$ and is due to a combination of effects: 1) the driving force is high, and the current is only increasing slowly, 2) the reaction rate at the back of the electrode goes through a maximum at a value of $I^* = 0.7273$ as discussed previously in Figure 4, and 3) the driving force, though high, is not large enough for the side reaction to contribute substantially to the ohmic potential drop. For larger values of $(\Phi_1 - \Phi_2)_{\alpha L}$, the ohmic potential drop decreases due to a decreasing rate of reaction at the back of the electrode. Thus, the depth of penetration of the reaction is decreasing at $I^* = 0.95$. This was shown clearly in Figure 4 as the primary reaction approaches the limiting current distribution.

The minimum in the ohmic potential occurs simultaneously with the minimum in the total reaction rate at the back of the electrode

$\left(di_2^*/dy\right)|_{\alpha L}$ . At this point the rate of the side reaction becomes significant, and the ohmic drop increases accordingly.

We wish to emphasize that the existence of a local maximum and local minimum is dependent on the physical parameters and operating conditions. For example, if the exchange current density for the side reaction were significantly larger relative to the primary reaction, the driving force required to make the side reaction occur to a significant extent would be much less. Thus instead of the ohmic potential drop exhibiting a local maximum due mainly to the effects of the primary reaction (or lack of effect of the side reaction), the side reaction becomes the controlling factor and $\Delta\Phi_2$ increases monotonically with increasing $(\Phi_1 - \Phi_2)_{\alpha L}$ .

Another way to achieve a similar result (using the same physical parameters) is to increase the ohmic potential drop by increasing the superficial velocity as shown in Figure 10. The reactor cannot be operated at even twice the superficial velocity without loss of the limiting current-plateau and a lack of a local maximum and a local minimum in the ohmic potential drop,which is due to extensive interference by the side reaction. In harmony with the quantitative design principles,[1] these calculations show that an increase in the superficial velocity increases the ohmic potential drop in the solution so that there is either excessive side reaction at the entrance to the porous electrode or a failure to maintain the limiting-current condition near the exit. A decrease in the feed concentration as shown in Figure 11 will also increase the side reaction relative

to the primary reaction and cause the limiting-current plateau to become less distinct. The ability to calculate the current distributions below the limiting current and in the presence of a side reaction permits one to determine the economically optimum operating conditions and even permissible operating conditions when the side reaction accounts for a substantial fraction of the total current, and there is a penalty for making the electrode thicker because the side reaction does not necessarily decrease with increasing distance through the electrode.

## Conclusion and Summary

A theoretical model for flow-through porous electodes has been described for the specific application to metal-ion removal from dilute streams. A new set of dimensionless parameters has been suggested from the analysis, which characterize the relative importance of the following physical phenomena within a flow-through porous electrode: axial diffusion and dispersion $(D')$, backward rate of the primary reaction $(P_1)$, ohmic potential drop $(P_2)$, forward $(P_3)$ and backward $(P_4)$ rates of the side reaction.

Satisfactory agreement between model predictions and experimental data on overall reactor performance and deposit distributions has been achieved.

The knowledge of distributions of current, potential, and concentration in the presence of a side reaction above and below the limiting-current of the primary reaction makes it possible to design and optimize an electrode system for the most economical removal of

metal ions. But this design may only be accomplished if there are sufficient experimental data. Most important are values for the specific interfacial area $a$, the mass-transfer coefficient $k_m$, and the exchange current densities for the primary reaction and the side reaction.

## Acknowledgment

This work was supported by the U.S. Energy Research and Development Administration.

## Appendix

To obtain a more accurate representation of the derivatives in equations 28 to 31 more of the physics needed to be incorporated in their dependence. This was done by considering the concentration distribution at the limiting current, which decreases exponentially with electrode thickness.[1,14] With this in mind, a new variable was defined:

$$\theta = e^{C} . \qquad [A-1]$$

Now apply this equation to the upstream boundary condition on the concentration (equation 30) to obtain

$$e^{C}\left(1 - D' \frac{dC}{dy}\right) = 1 . \qquad [A-2]$$

Next introduce the central-difference approximations at the first real mesh point (j = 2 , mesh point 1 is an image point):

$$\theta_2\left(1 - D' \frac{C_3 - C_1}{2h}\right) = 1 , \qquad [A-3]$$

or

$$\theta_2\left(1 - \frac{D'}{2h} \ln \frac{\theta_3}{\theta_1}\right) = 1 . \qquad [A-4]$$

If $\theta$ is approximately exponential in distance, then $C$ will be approximately linear, and less error will be introduced when the derivative is approximated by a finite-difference form in the variable $C$.

Similarly, a central-difference approximation for the axial diffusion and axial dispersion term in equation 28 can be derived for any interior mesh point $j$

$$D' \frac{d^2\theta}{dy^2} = \frac{D'\theta_j}{h^2}\left[\frac{1}{4}\left(\ln \frac{\theta_{j+1}}{\theta_{j-1}}\right)^2 + \ln\left(\frac{\theta_{j+1}\theta_{j-1}}{\theta_j^2}\right)\right] . \qquad [A-5]$$

The resulting material balance equation at any interior mesh point $j$ now becomes

$$\frac{\theta_j}{2h} \ln \frac{\theta_{j+1}}{\theta_{j-1}} = \frac{D'\theta_j}{h^2}\left[\frac{1}{4}\left(\ln \frac{\theta_{j+1}}{\theta_{j-1}}\right)^2 + \ln\left(\frac{\theta_{j+1}\theta_{j-1}}{\theta_j^2}\right)\right] - J_{Rj} \qquad [A-6]$$

where

$$J_{Rj} = \frac{\theta_j - P_1 e^{(\alpha_{aR}/\alpha_{cR}+1)\eta'_j}}{1 + e^{\eta'_j}} . \qquad [A-7]$$

To check <u>a posteriori</u> the overall application of Faraday's law, whereby the integral of the transfer current $J_R$ for the principal reaction

should be related to the difference between the inlet and outlet concentrations of the principal reactant, one should use an integration formula for $J_R$ which also takes account of the approximately exponential dependence of $J_R$ on distance.

So that the integrated current is also correct for the side reaction, combine equations 28 and 29 by eliminating $J_R$ from both equations to yield

$$\frac{d}{dy}\left(\frac{1}{P_2}\frac{d\eta'}{dy} + \theta - D'\frac{d\theta}{dy}\right) = J_S \ , \qquad [A-8]$$

where

$$J_S = P_3 \exp\left(-\alpha_{cS}\eta'/\alpha_{cR}\right)\left[1 - P_4 \exp\left(\frac{\alpha_{aS} + \alpha_{cS}}{\alpha_{cR}}\eta'\right)\right] . \qquad [A-9]$$

Next express the outer-derivative in equation A-8 as a central-difference written between points halfway between mesh points:

$$\frac{1}{h}\left[\left(\frac{1}{P_2}\frac{d\eta'}{dy} + \theta - D'\frac{d\theta}{dy}\right)_{j+\frac{1}{2}} - \left(\frac{1}{P_2}\frac{d\eta'}{dy} + \theta - D'\frac{d\theta}{dy}\right)_{j-\frac{1}{2}}\right] = J_S \ . \qquad [A-10]$$

Now express the terms $\theta - D'd\theta/dy$ halfway between two mesh points using equation A-1 and the values of $\theta$ at the adjacent mesh points (see also equation A-2):

$$\left(\theta - D'\frac{d\theta}{dy}\right)_{j+\frac{1}{2}} = \sqrt{\theta_j\theta_{j+1}}\left(1 - \frac{D'}{h}\ln\frac{\theta_{j+1}}{\theta_j}\right) , \qquad [A-11]$$

and

$$\left(\theta - D' \frac{d\theta}{dy}\right)_{j-\frac{1}{2}} = \sqrt{\theta_j \theta_{j-1}} \left(1 - \frac{D'}{h} \ln \frac{\theta_j}{\theta_{j-1}}\right) . \qquad [A-12]$$

With these approximations and a central-difference expression for the derivative of $\eta'$ , the resulting equation for the potential at any interior mesh point $j$ becomes

$$\frac{1}{P_2} \frac{\eta'_{j+1} + \eta'_{j-1} - 2\eta'_j}{h^2} + \frac{\sqrt{\theta_j \theta_{j+1}}}{h} \left(1 - \frac{D'}{h} \ln \frac{\theta_{j+1}}{\theta_j}\right) - \frac{\sqrt{\theta_j \theta_{j-1}}}{h} \left(1 - \frac{D'}{h} \ln \frac{\theta_j}{\theta_{j-1}}\right)$$

$$= J_{Sj} . \qquad [A-13]$$

Similarly, to treat the upstream boundary condition for the potential, integrate equation A-8 from zero to $h/2$ to yield

$$\left(\frac{1}{P_2} \frac{d\eta'}{dy} + \theta - D' \frac{d\theta}{dy}\right)_{h/2} - \left(\frac{1}{P_2} \frac{d\eta'}{dy} + \theta - D' \frac{d\theta}{dy}\right)_o = \frac{h}{2} J_{Sj} . \qquad [A-14]$$

Use the same approximations as above for $y = h/2$ and use the boundary conditions in equation 30 to obtain (for $j = 2$)

$$\frac{2}{h} \frac{1}{P_2} \frac{\eta'_{j+1} - \eta'_j}{h} + \frac{2}{h} \sqrt{\theta_j \theta_{j+1}} \left(1 - \frac{D'}{h} \ln \frac{\theta_{j+1}}{\theta_j}\right) - \frac{2}{h} \left(\frac{P_5}{P_2} I^* + 1\right) = J_{Sj} . \qquad [A-15]$$

With equation A-13 at the interior mesh points, this corresponds then to a trapezoidal integration of the transfer current $J_S$ over the thickness of the porous electrode.

The governing finite-difference equations A-6 and A-13 along with the upstream boundary conditions A-4 and A-15 were then linearized about a trial solution and solved simultaneously with the downstream boundary condition for $\theta$ and $\eta'$ using Newman's technique.[23] The new approximations to the derivatives in concentration provided accurate values for $\theta$ and $\eta'$ at the mesh points without introducing anomalous values for the integrated current.

## Notation

| | |
|---|---|
| $a$ | specific interfacial area, $cm^{-1}$ |
| $B$ | see equation 47 |
| $C$ | $= \ln \theta$ |
| $c_R$ | concentration of metal-ion reactant, $mole/cm^3$ |
| $c_{Rf}$ | upstream feed concentration of metal-ion reactant, $mole/cm^3$ |
| $c_{Rw}$ | wall concentration of metal-ion reactant |
| $c_S$ | hydrogen ion concentration, $mole/cm^3$ |
| $D_a$ | axial dispersion coefficient of metal-ion reactant, $cm^2/s$ |
| $D_o$ | molecular diffusion coefficient of metal-ion reactant, $cm^2/s$ |
| $D_R$ | effective diffusion coefficient of metal ion reactant, $cm^2/s$ |
| $D'$ | dimensionless parameter describing the relative importance of axial diffusion and dispersion, see equation 32 |
| $F$ | Faraday's constant, 96487 C/equiv |
| $h$ | dimensionless distance between mesh points |

$i$ superficial current density to an electrode, $A/cm^2$

$i_{oj}$ exchange current density for reaction $j$, $A/cm^2$

$i_{oj,ref}$ exchange current density for reaction $j$ at a reference composition $c_{i,ref}$, see equation 14, $A/cm^2$

$i_1$ superficial current density in the matrix, $A/cm^2$

$i_2$ superficial current density in pore-solution phase, $A/cm^2$

$i_{nj}$ transfer current for reaction $j$ per unit interfacial area, $A/cm^2$

$I^*$ dimensionless superficial current density to an electrode, see equation 41

$i_2^*$ dimensionless current density in pore-solution phase, see equation 61

$i_2^*(o)$ $= -I^*$ total dimensionless current density in pore-solution phase, see equation 48

$i_R$ total current density to an electrode due to metal-deposition reaction, $A/cm^2$

$I$ total current to an electrode, A

$j_{in}$ pore-wall flux of species i, $mole/cm^2\text{-}s$

$J_R$ dimensionless transfer current of metal deposition reaction, see equation A-6

$J_S$ dimensionless transfer current of side reaction, see equation A-9

$k_m$ average mass-transfer coefficient between flowing solution and electrode surface, cm/s

$L$ thickness of porous electrode, cm

$M_i$ symbol for the chemical formula of species i

$n$ number of electrons transferred in metal deposition reaction

$n_j$ number of electrons transferred in reaction j

$N_R$ superficial flux of metal-ion reactant, mole/$cm^2$-s

$p_S$ hydrogen partial pressure, atm

Pe Péclet number, $v/aD_o$

$P_1$ dimensionless parameter describing the relative importance of the backward term in the metal deposition reaction, see equation 34

$P_2$ dimensionless parameter describing the relative importance of the ohmic potential drop, see equation 35

$P_3$ dimensionless parameter describing the relative importance of the forward term in the side reaction, see equation 36

$P_4$ dimensionless parameter describing the relative rate of the backward term in the side reaction, see equation 37

$P_5$ dimensionless parameter which characterizes the ohmic potential drop in the pore-solution phase, see equation 38

$P_6$ dimensionless parameter which characterizes the ohmic potential drop in the matrix phase, see equation 39

$q_{ij}$ cathodic reaction order

R universal gas constant, 8.3143 J/mole-K

$s_{ij}$ stoichiometric coefficient of species i in electrode reaction j

$s_R$ stoichiometric coefficient of metal-ion reactant

T absolute temperature, K

$U_{jw}$ open-circuit potential for reaction j at local wall composition relative to a reference electrode of a given kind, V, see equation 17

$U_j^\theta$ standard electrode potential for reaction j, V

$U_r^\theta$ standard electrode potential of reference electrode, V

$\Delta U$ $= U_S - U_R$ difference in open-circuit cell potentials of the side reaction and primary reaction at the reference composition, V

v superficial fluid velocity, cm/s

VOP potential of the cathode current collector relative to a saturated calomel reference electrode placed in the dilute product stream, V

x distance through porous electrode, cm

y $x\, ak_m/v$ dimensionless distance through porous electrode

$z_i$ valance or charge number of species i

Greek letters

$\alpha$ $= a\, k_m/v$, reciprocal of penetration depth at the limiting current, $cm^{-1}$

$\alpha_{aj}$ anodic transfer coefficient for reaction j

$\alpha_{cj}$ cathodic transfer coefficient for reaction j

$\gamma_{ij}$ exponent in composition dependence of exchange current density

$\varepsilon$ porosity or void volume

$\eta_{sj}$ $= \Phi_1 - \Phi_2 - U_{jw}$ surface overpotential for reaction j, V

$\eta$ $= \Phi_1 - \Phi_2$ local overpotential, V

$\eta'$ dimensionless local overpotential, see equation 33

$\kappa$ effective conductivity of solution, mho/cm

$\kappa_o$ intrinsic conductivity of solution, mho/cm

$\nu$ kinematic viscosity of solution, $cm^2/s$

$\rho_o$ density of pure solvent, $Kg/cm^3$

$\sigma$ effective conductivity of solid matrix, mho/cm

$\psi$ dimensionless particle shape factor (= 0.86 for flakes)

$\Phi_1$ electrostatic potential in matrix phase, V

$\Phi_2$ quasi-electrostatic potential in the pore solution phase, V

$\Delta\Phi_2$ ohmic potential drop across porous electrode, V

$\Delta\Phi_2'$ estimate of ohmic potential across porous electrode at the limiting current, V, see equation 49

$\tau$ tortuosity factor

$\theta$ $= c_R/c_{Rf}$, dimensionless concentration of metal-ion reactant

Subscripts

r reference electrode compartment

R metal-ion reactant or primary reaction

ref reference composition

S side reactant or side reaction

w wall or electrode surface

## References

1. Douglas N. Bennion and John Newman. "Electrochemical removal of copper ions from very dilute solutions." Journal of Applied Electrochemistry, 2, 113-122 (1972).

2. R. S. Wenger, D. N. Bennion, and J. Newman. "Electrochemical Concentrating and Purifying from Dilute Copper Solutions." Abstract 236, Chicago meeting. Journal of the Electrochemical Society, 120, 1096 (1973).

3. Robert S. Wenger. Electrical Concentrating and Purifying from Dilute Copper Solutions. M. S. Thesis. Los Angeles: University of California, 1974.

4. F. A. Posey. Electrolytic Demonstration Unit for Copper Removal from Distillation Plant Blowdown. ORNL-TM-4112. Oak Ridge: Oak Ridge National Laboratory, 1973.

5. A. T. Kuhn and R. W. Houghton. "Antimony removal from dilute solutions using a restrained bed electrochemical reactor." Journal of Applied Electrochemistry, 4, 69-73 (1974).

6. J. M. Williams and K. B. Keating. "Extended-Surface Electrolysis Removes Heavy Metals from Waste Streams." Dupont Inovation, 6 (no. 3), 6-10 (1975).

7. A. K. P. Chu, M. Fleischmann, and G. J. Hills. "Packed bed electrodes. I. The electrochemical extraction of copper ions from dilute aqueous solutions." Journal of Applied Electrochemistry, 4, 323-330 (1974).

8. John Van Zee and John Newman. "Electrochemical Removal of Silver Ions from Photographic Fixing Solutions Using a Porous Flow-Through Electrode." Journal of the Electrochemical Society, to be published.

9. R. D. Armstrong, O. R. Brown, R. D. Giles, and J. A. Harrison. "Factors in the Design of Electrochemical Reactors." Nature, 219, 94 (1968).

10. G. Kreysa, S. Piontech, and E. Heitz. "Comparative investigations of packed and fluidized bed electrodes with non-conducting and conducting particles." Journal of Applied Electrochemistry, 5, 305-312 (1975).

11. A. T. Kuhn and R. W. Houghton. "A Comparison of the Performance of Electrochemical Reactor Designs in the Treatment of Dilute Solutions." Electrochimica Acta, 19, 733-737 (1974).

12. John Newman and William Tiedemann. "Porous-Electrode Theory with Battery Applications." AIChE Journal, 21, 25-41 (1975).

13. Richard Alkire and Brian Gracon. "Flow-Through Porous Electrodes." Journal of the Electrochemical Society, 122, 1594-1601 (1975).

14. John Newman and William Tiedemann. "Flow-Through Porous Electrodes." Advances in Electrochemistry and Electrochemical Engineering, in press.

15. R. E. Sioda. "The ECE Mechanism in Flow Electrolysis in Porous Electrodes Under Conditions of Limiting Current." Electrochimica Acta, 20, 457-461 (1975).

16. R. E. Sioda. "Current-Potential Dependence in the Flow Electrolysis on a Porous Electrode." Journal of Electroanalytical Chemistry and Interfacial Electrochemistry, 34, 399-409 (1972).

17. Richard Alkire and Ronald Gould. "Analysis of Multiple Reaction Sequences in Flow-Through Porous Electrodes." Journal of the Electrochemical Society, 123, 1842-1849 (1976).

18. B. G. Ateya and L. G. Austin. "Steady-State Polarization at Porous, Flow-Through Electrodes with Small Pore Diameter. I. Reversible Kinetics." Journal of the Electrochemical Society, 124, 83-89 (1977).

19. P. V. Danckwerts. "Continuous Flow Systems. Distribution of Residence Times." Chemical Engineering Science, 2, 1-13 (1953).

20. J. F. Wehner and R. H. Wilhelm. "Boundary Conditions of Flow Reactor." Chemical Engineering Science, 6, 89-93 (1956).

21. Thomas K. Sherwood, Robert L. Pigford, and Charles R. Wilke, Mass Transfer, New York, McGraw-Hill (1975), p. 136.

22. R. E. de la Rue and C. W. Tobias. "On the Conductivity of Dispersions." Journal of the Electrochemical Society, 106, 827 (1959).

23. John Newman Electrochemical Systems, Prentice-Hall, Englewood Cliffs, N.J. (1973). p. 177, Appendix C.

24. E. J. Wilson and C. J. Geankoplis. "Liquid Mass Transfer at Very Low Reynolds Numbers in Packed Beds." Industrial and Engineering Chemistry Fundamentals, 5, 9-14 (1966).

25. R. Byron Bird, Warren E. Stewart, and Edwin N. Lightfoot. Transport Phenomena, Wiley, New York, 1960, pp. 411-412.

26. Peter W. Appel and John Newman. "Application of the Limiting-Current Method to Mass Transfer in Packed Beds at Very Low Reynolds Numbers." AIChE Journal, 22, 979-984 (1976).

27. Tibor Erdez-Gruz, Kinetics of Electrode Processes, Wiley-Interscience, New York (1972), pp. 165.

28. Douglas N. Bennion. "Flow Through Porous Electrodes for Removal of Ions from Dilute Solutions." Abstract 69. Zurich meeting. International Society of Electrochemistry (1976).

29. J. Euler, and W. Nonnenmacher. "Stromverteilung in porösen Electroden." Electrochimica Acta, 2, 268 (1960).

30. John S. Newman and Charles W. Tobias. "Theoretical Analysis of Current Distribution in Porous Electrodes." Journal of the Electrochemical Society, 109, 1183 (1962).

31. James A. Trainham and John Newman. "A Thermodynamic Estimation of the Minimum Concentration Attainable in a Flow-Through Porous Electrode Reactor." Journal of Applied Electrochemistry, to be published.

This report was done with support from the United States Energy Research and Development Administration. Any conclusions or opinions expressed in this report represent solely those of the author(s) and not necessarily those of The Regents of the University of California, the Lawrence Berkeley Laboratory or the United States Energy Research and Development Administration.

*TECHNICAL INFORMATION DIVISION*
*LAWRENCE BERKELEY LABORATORY*
*UNIVERSITY OF CALIFORNIA*
*BERKELEY, CALIFORNIA 94720*